Room Temperature Frenkel-Wannier-Mott Hybridization of Degenerate Excitons in a Strongly Coupled Microcavity

Michael Slootsky,[1] Xiaoze Liu,[2] Vinod M. Menon,[2,*] and Stephen R. Forrest[1,3,*]
[1]*Department of Physics, University of Michigan, Ann Arbor, Michigan 48109, USA*
[2]*Department of Physics, Graduate Center, and Department of Physics, Queens College, City University of New York, New York, New York 11367, USA*
[3]*Department of Electrical Engineering and Computer Science, and Department of Materials Science and Engineering, University of Michigan, Ann Arbor, Michigan 48109, USA*
(Received 15 September 2013; published 18 February 2014)

Hybrid organic-inorganic polaritons are formed by the simultaneous strong coupling of two degenerate excitons and a microcavity photon at room temperature. Wannier-Mott and Frenkel excitons in spatially separated ZnO and 3,4,7,8-napthalene tetracarboxylic dianhydride (NTCDA) layers, respectively, placed in a single Fabry-Perot microcavity contribute to the interaction with the cavity. A Rabi splitting of (322 ± 8) meV between the upper and middle branches of the three branch polariton energy-momentum dispersion is observed. This is compared to only (224 ± 22) meV and (218 ± 8) meV Rabi splittings for NTCDA-only and ZnO-only reference cavities, respectively, and indicates that the excitonic component of the polariton is a Frenkel-Wannier-Mott hybrid. Unlike previous reports of hybrid polaritons, the mixing of the organic and inorganic eigenstates occurs independently of angle due to their energetic degeneracy, and can be tailored by adjusting the optical field distribution within the cavity.

DOI: 10.1103/PhysRevLett.112.076401 PACS numbers: 71.36.+c, 42.70.Jk, 78.67.Bf

For a number of years, combining organic and inorganic semiconductor systems has been of interest as a means to precisely engineer optoelectronic properties to meet the requirements of particular applications [1–3]. Hybrid structures using direct Coulomb coupling of tightly bound and stable organic Frenkel, and more delocalized and unstable (at room temperature) inorganic Wannier-Mott (WM) excitons have been sought to produce efficient nonradiative energy transfer, enhanced oscillator strength, and optical nonlinearities [4–13]. Because of the limited range of the dipole-dipole interaction, however, a more convenient approach to hybridization of these remarkably dissimilar excited states is photon-mediated coupling in a microcavity [14]. In the limit of strong light-matter coupling (i.e., when the interaction strength exceeds the excitonic and cavity linewidths), formation of new quasiparticle eigenstates, known as polaritons, has been demonstrated by mixing multiple excitons with a cavity photon [15–19]. In the case of nonresonant excitons, the contribution of each component (and thus the excitonic hybridization) varies with angle [20]. Here, we demonstrate uniform Frenkel-Wannier-Mott hybridization of degenerate excitons in spatially separate nanoparticle ZnO and 3,4,7,8-napthalene tetracarboxylic dianhydride (NTCDA) layers within a strongly coupled microcavity. Remarkably, these hybrid states are stable at room temperature, which differs from previous reports of organic and inorganic polaritons that were only observed well below 300 K. Their stability and angle independence opens up new possibilities for the use of hybrid systems in practical optoelectronic and nonlinear optical applications.

In the strong-coupling regime, the new normal modes of the system possess both excitonic and photonic character. The intersecting energy-momentum dispersions of the uncoupled photon and exciton(s) split into anticrossing polariton branches. The number of branches is equal to the number of interacting photonic and excitonic states. The energy separation between the branches around each excitonic resonance, known as the Rabi splitting, is proportional to the strength of the light-matter interaction, which in turn depends on the oscillator strength of the materials. Because of conservation of the in-plane momentum associated with the photonic component of the polariton, the dispersion can be observed in angle-resolved reflectivity or (when present) photoluminescence with a one-to-one mapping between angle and polariton in-plane momentum. In general, the proportion of the photon and exciton contributions to the polariton varies along each branch. In previously reported hybrid organic or inorganic polariton systems [17–19], the Rabi splitting was smaller than the energy difference between Frenkel and WM excitons resulting in three branches, the middle branch consisting of both excitons and the photon. Thus, the ratio of the organic to the inorganic exciton contribution varied with angle for the hybrid middle polariton. A theoretical treatment of such resonant (but *nondegenerate*) hybrid systems has been previously developed [20]. In this work, we focus on degenerate Frenkel and WM excitons that simultaneously couple to the cavity mode, thereby behaving as a

single, angle-independent hybridized excitonic component of the resulting polaritons.

Three microcavities, shown schematically in Fig. 1, were prepared for this study employing (a) inorganic semiconductor ZnO nanoparticles, (b) small-molecular weight organic NTCDA, and (c) both as active materials. The bottom mirror, a distributed Bragg reflector (DBR) consisting of 8.5 pairs of SiO_2/SiN_x, was deposited directly onto precleaned quartz by plasma-enhanced chemical vapor deposition. Optical constants were measured using variable-angle spectroscopic ellipsometry, and DBR layer thicknesses were adjusted to produce mirrors with a center wavelength around $\lambda = 380$–390 nm. Approximately 175-nm-thick ZnO films were spin coated onto the DBR from a ZnO nanoparticle (<35 nm average diameter) dispersion (Sigma-Aldrich SKU#721085) diluted by ethanol to ~9.6 wt %. The films were subsequently baked in air at 300 °C for 10 min. to drive off the solvent. 60-nm-thick NTCDA films were thermally deposited in high vacuum (base pressure $<5 \times 10^{-7}$ Torr) by sublimation from a resistive source. The silica (SiO_2) spacer was deposited using *e*-beam thermal evaporation. The active layers were capped by a partially transparent, 10-nm-thick *e*-beam evaporated Al mirror. Angle and spectrally resolved cavity reflectivity was measured at room temperature from the Al side using TE-polarized light to probe the energy-momentum dispersion of the cavities with 2.5 nm and 2.5° resolution.

The optical constants of the ZnO nanoparticles and NTCDA measured on Si by spectroscopic ellipsometry and fit by a generalized oscillator model are shown in Fig. 1(d). NTCDA has two pronounced absorption peaks corresponding to the lowest-energy exciton ($E_{00} \approx 3.18$ eV) and its vibronic 0-1 exciton replica ($E_{01} \approx 3.38$ eV). The higher-energy vibronic is approximately resonant with the ZnO exciton ($E_{\mathrm{ZnO}} \approx E_{01}$) which is partly obscured by the band-edge absorption but is stable at room temperature due to its high binding energy of roughly 60 meV. For convenience, exciton energies will henceforth be referred to as $E_1 = E_{00}$ and $E_2 = E_{01} = E_{\mathrm{ZnO}}$ for the lower- and higher-energy excitons, respectively. Compared to bulk ZnO, the nanoparticle film has a slightly reduced refractive index and optical absorption, likely owing to reduced density of the spin-coated layer. Nonetheless, the film is optically homogeneous and, as apparent in Fig. 1(d), has an absorption peak intensity roughly half that of the higher-energy exciton in NTCDA. To compensate for its lower oscillator strength, the cavity structure was designed such that two electric field antinodes are located in the ZnO layer and one in NTCDA. The thickness of the silica spacer (used to prevent direct coupling of the excited states in these two materials) was optimized for a negative detuning, i.e., the energy of the photon mode at normal incidence, $E_0 = E_{\mathrm{ph}}(\theta = 0°)$, is below the higher-energy excitons ($E_0 < E_2$). A transfer

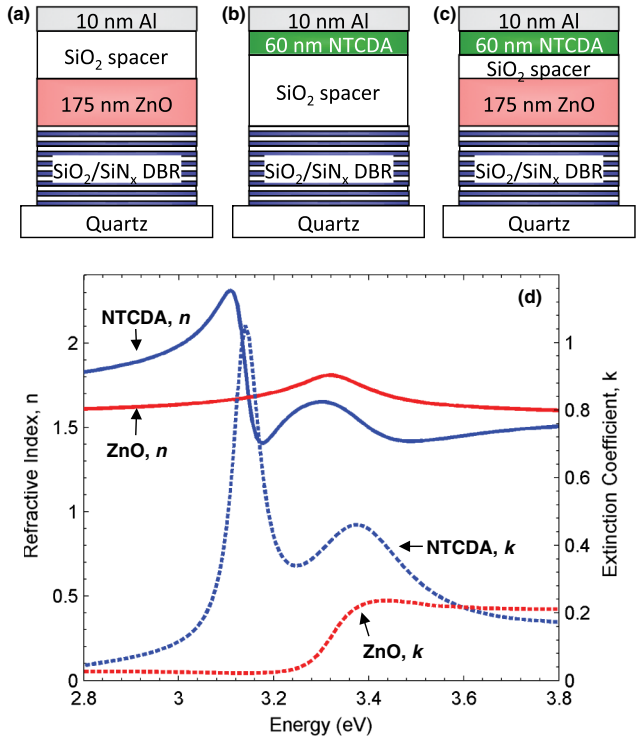

FIG. 1 (color online). The structure of the strongly coupled (a) ZnO, (b) NTCDA, and (c) hybrid cavities. The SiO_2 spacer thickness is adjusted between the three structures to maintain similar detuning. (d) Refractive index (*n*, solid lines) and extinction coefficient (*k*, dotted lines) of ZnO and NTCDA on Si measured by ellipsometry. The ZnO absorption is roughly half that of the 0-1 vibronic of NTCDA.

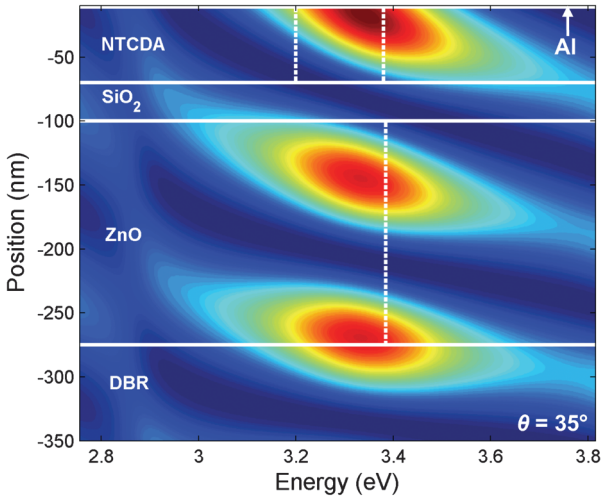

FIG. 2. (color). Optical field distribution in the hybrid optical microcavity. Transfer matrix simulations determine the optical field intensity as a function of position in the cavity. The cavity mode is nearly resonant with the 0-1 NTCDA and ZnO excitons at $\theta = 35°$. Solid lines indicate layer boundaries, dashed lines indicate approximate position of the excitons. Note that although the 10-nm Al layer is too thin to see in the figure, it is included in the simulation.

matrix simulation of the optical field intensity in the hybrid cavity is shown in Fig. 2 for $\theta = 35°$, approximately where the uncoupled cavity dispersion crosses E_2. In the ZnO-only and NTCDA-only cavities, the spacer thickness was increased to compensate for the optical length of the missing active layer, thereby maintaining comparable detunings and field distributions in all samples.

In the case of the single ZnO exciton coupled to the cavity, two polariton branches are formed, while the two coupled vibronics of NTCDA result in a complex, multibranch energy-momentum dispersion. Figure 3 shows the room-temperature TE-polarized reflectivity of strongly coupled ZnO, NTCDA, and hybrid cavities. As expected, the ZnO cavity has two features: the lower polariton is photonlike at near normal ($\theta = 0°$) incidence and is increasingly excitonlike at higher angles. The upper branch is difficult to resolve due to the broadband absorption of ZnO above the uncoupled exciton energy. As evident in Fig. 3(d), rather than producing a distinct reflectivity minimum, the upper polariton appears as a shoulder at low incidence angles, turning into a shallow and rather broad feature at higher angles. Equal photon-exciton mixing is achieved at the point of anticrossing for both polariton branches (Fig. 3 inset). The three-branch dispersion observed in NTCDA and hybrid cavities indicates that two excitons are strongly coupled to the photon in both cases. The hybrid cavity, however, has an increased splitting between the upper and middle polariton branches. In fact, the Rabi splitting around E_2 in the hybrid cavity exceeds that of ZnO and NTCDA, suggesting that both excitons are strongly coupled and jointly contribute to the oscillator strength of the E_2 transition.

The polariton dispersion extracted from the reflectivity minima [Figs. 3(a)–3(c), filled circles] can be fit by a coupled three-oscillator Hamiltonian [15,20,21] given by

$$\begin{bmatrix} E_{\mathrm{ph}} & V_1 & V_2 \\ V_1 & E_1 & 0 \\ V_2 & 0 & E_2 \end{bmatrix} \begin{bmatrix} \alpha \\ \beta \\ \gamma \end{bmatrix} = \varepsilon \begin{bmatrix} \alpha \\ \beta \\ \gamma \end{bmatrix}, \tag{1}$$

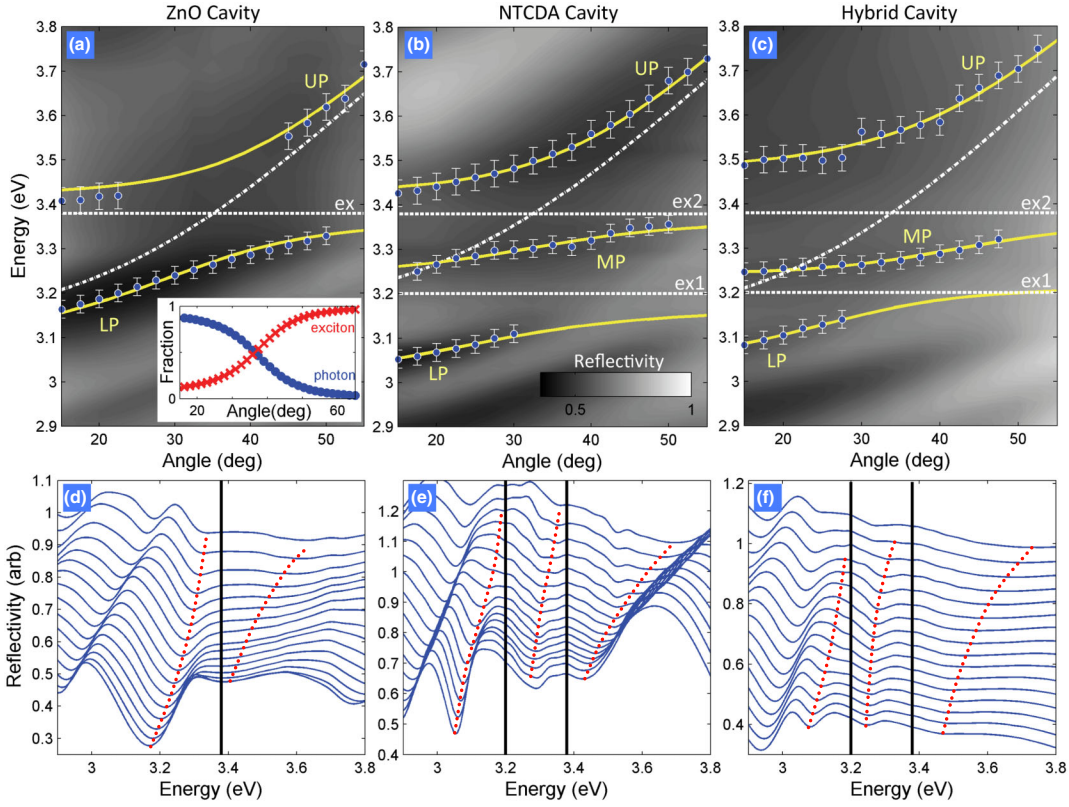

FIG. 3 (color online). Room-temperature angle-resolved TE-polarized reflectivity (gradient) is measured for the (a),(d) ZnO, (b),(e) NTCDA, and (c),(f) hybrid cavities. As expected, three polariton branches (upper, middle, and lower) are observed in (b),(e) and (c),(f), while only two (upper and lower) are observed in (a),(d). In (a)–(c), the extracted minima of the reflectivity (filled circles) highlight the positions of the polariton branches, while the solid lines correspond to a coupled-oscillator Hamiltonian fit with parameters as listed in Table I. For reference, the uncoupled cavity mode (dash-dotted) and exciton energies (dashed) are also indicated. In (d)–(f), vertical lines indicate positions of excitons, dotted lines show approximate positions of the polariton features. Inset: Photonic (circles) and excitonic (crosses) fraction of the lower polariton branch in (a) extracted from the two-oscillator fit. In the upper branch, the photon and exciton fractions are exactly reversed.

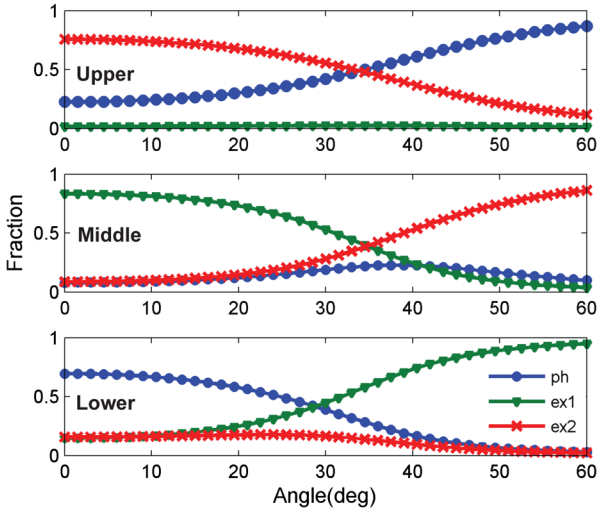

FIG. 4 (color online). Hopfield coefficients showing the composition of the upper, middle, and lower polaritons in the hybrid cavity extracted from the Hamiltonian fit. The upper branch is composed largely of the uniformly hybridized (ZnO/NTCDA 0-1) exciton (ex2, crosses) and photon (circles). The lower branch is mostly NTCDA 0-0 exciton (ex1, triangles) mixed with the photon. The middle branch contains all three components.

where E_{ph} is the cavity mode dispersion, V_1 and V_2 are interaction potentials between the photon and excitons, α^2, β^2, and γ^2 are the Hopfield mixing coefficients representing the fractional contribution of each component (Fig. 4), and ε are angle-dependent polariton eigenenergies [Figs. 3(a)–3(c), solid lines]. For the ZnO cavity, V_1 and E_1 are omitted and the Hamiltonian is reduced to two coupled oscillators. The cavity dispersion is approximated by $E_{\mathrm{ph}}(\theta) = E_0(1 - \sin^2\theta/{n_{\mathrm{eff}}}^2)^{-(1/2)}$ where E_0 is the cavity cutoff energy as before, and n_{eff} is the effective refractive index of the cavity that takes into account field penetration into the bottom distributed Bragg reflector (DBR) and index differences between the active and spacer layers. The magnitude of the Rabi splitting is proportional to twice the interaction energy, i.e., $\Omega_i = 2V_i$. Using V_i, E_0, n_{eff} as fitting parameters, we extract Rabi splittings of (322 ± 8), (224 ± 22), and (218 ± 8) meV between the upper two branches in the hybrid, NTCDA and ZnO cavities, respectively. The values of all parameters are listed in Table I.

The greatly enhanced interaction potential V_2 in the hybrid cavity indicates stronger photon-exciton coupling compared to that in "pure" cavities. This enhancement, in contrast to previous reports [17–19] on hybrid polaritons, can result from improved electric field overlap with the active layers, increased cavity quality and/or greater total oscillator strength. Since the detuning and overall optical length is kept roughly equal in all three cavities, the field distribution has only negligible variation. Likewise, because the structures all share the same mirrors, only minor differences in cavity quality are expected. Therefore, the hybrid cavity dispersion is consistent with increased oscillator strength of the E_2 exciton which, in the present case, is a hybrid of the Wannier-Mott and Frenkel excitons. The observed enhancement in the Rabi splitting of the hybrid cavity by a factor of (1.44 ± 0.15) compared to that of the pure NTCDA cavity conclusively shows that indeed both the Frenkel excitons in NTCDA and Wannier-Mott excitons in ZnO simultaneously strongly couple to the photon mode, and together contribute to the strength of the E_2 transition.

In previous work, hybridization of two nonresonant excitons and a photon occurred predominantly in the middle polariton branch [17–19]. Since the excitonic fractions in the middle polariton must vary with wave vector [20] (as in Fig. 4), equal and maximum mixing of the excitons occurs at only a single incidence angle. Moreover, the photon contribution at this maximum is also significant. In the hybrid cavity reported here, the degenerate ZnO and NTCDA excitons are indistinguishably strongly coupled at all angles, acting as a single hybrid exciton ("ex2" in Fig. 4) with the combined oscillator strengths of the two active layers. Therefore, the hybridization of NTCDA 0-1 and ZnO excitons is independent of the Hopfield mixing coefficients, instead resulting from the field overlap with the active layers which can be tailored by adjusting their thicknesses. Indeed, it is not possible to extract the individual contributions of the degenerate excitons using this formalism. The properties of the upper branch (which consists almost exclusively of the Frenkel-Wannier-Mott hybrid exciton mixed with the cavity photon) and the middle branch (which also adds the NTCDA 0-0 vibronic into the mix) are expected to be significantly different from either semiconductor. Unfortunately, the presence of the 0-0 exciton also means that upon excitation, the polariton population quickly relaxes to the lower branch via emission

TABLE I. Parameters for the coupled-oscillator model used to fit polariton dispersions of the ZnO, NTCDA, and hybrid cavities. For the ZnO case, a two-level Hamiltonian is used since only one exciton is present. Best fits were obtained using $E_1 = 3.2$ eV and $E_2 = 3.38$ eV. Mirrors consist of an 8.5 pair SiO_2/SiN_X DBR, and a 10-nm-thick Al cap.

Cavity structure	E_0 (eV)	n_{eff}	V_1 (meV)	V_2 (meV)
175 nm ZnO/90 nm SiO_2	3.17 ± 0.01	1.65 ± 0.04		109 ± 4
115 nm SiO_2/60 nm NTCDA	3.15 ± 0.03	1.6 ± 0.08	111 ± 4	112 ± 11
175 nm ZnO/35 nm SiO_2/60 nm NTCDA	3.17 ± 0.02	1.6 ± 0.04	75 ± 8	161 ± 4

of a molecular phonon. For this reason, no photoluminescence is observed from the middle or upper branches (see Supplemental Material [22]). The lower polariton photoluminescence generally follows the dispersion observed in reflectivity, but due to only minor contributions from the hybrid exciton, it yields little insight into the hybridization. A more convenient system would consist of an organic-inorganic microcavity where participation is limited to only degenerate excitons. Alternatively, a system with degeneracy between the hybrid polariton and the emission from the lowest molecular vibronic could be used to achieve fast population transfer to the bottom of the lower polariton branch, bypassing the bottleneck that often impedes polariton lasing in inorganic systems.

In summary, degenerate Frenkel and Wannier-Mott excitons are hybridized within an optical microcavity in the strong-coupling regime. The hybrid polariton states are stable at room temperature. A characteristic polariton dispersion and an increased Rabi splitting of (322 ± 8) meV is observed in angle-resolved reflectivity of a cavity containing NTCDA and ZnO as active materials confirming strong coupling of both species. The splitting is larger than that of comparably detuned cavities containing only NTCDA or ZnO, and suggests that the two semiconductors are acting as a single, uniformly hybridized excitonic component of the resulting polariton eigenstate. The upper polariton consists of a mixture of the hybrid exciton and cavity photon, while for the middle polariton, these states are further hybridized with the nondegenerate NTCDA 0-0 exciton. In contrast to previous work, the Frenkel-Wannier-Mott hybridization does not vary as a function of in-plane momentum for the upper branch, and only varies in the middle branch due to the presence of a second nonresonant Frenkel state. Because of significant contributions from the hybrid exciton, both the upper and middle polariton branches are expected to have novel optical properties (e.g., pronounced third-order nonlinear optical susceptibility [3]) that warrant further investigation. Although the population dynamics of the NTCDA/ZnO polariton system are dominated by fast relaxation to the lowest branch via emission of an intermolecular phonon in NTCDA, such hybrid degenerate systems nonetheless offer a promising pathway to nonlinear devices with engineered optical properties.

The authors thank Hui Deng for useful discussions, and the National Science Foundation (Grant No. DMR 1105392) for financial support. Sample fabrication was done in part at the University of Michigan Lurie Nanofabrication Facility. M. S. and X. L. contributed equally to this work.

*Corresponding authors.
vmenon@qc.cuny.edu
stevefor@umich.edu

[1] S. R. Forrest, M. L. Kaplan, P. H. Schmidt, W. L. Feldmann, and E. Yanowski, Appl. Phys. Lett. **41**, 90 (1982).
[2] N. Li, K. Lee, C. K. Renshaw, X. Xiao, and S. R. Forrest, Appl. Phys. Lett. **98**, 053504 (2011).
[3] V. M. Agranovich, Y. N. Gartstein, and M. Litinskaya, Chem. Rev. **111**, 5179 (2011).
[4] G. C. L. Rocca, F. Bassani, and V. M. Agranovich, Nuovo Cimento Soc. Ital. Fis. **17D**, 1555 (1995).
[5] A. Engelmann, V. I. Yudson, and P. Reineker, Phys. Rev. B **57**, 1784 (1998).
[6] Y. Gao, N. Q. Huong, J. L. Birman, and M. J. Potasek, J. Appl. Phys. **96**, 4839 (2004).
[7] S. Blumstengel, S. Sadofev, C. Xu, J. Puls, and F. Henneberger, Phys. Rev. Lett. **97**, 237401 (2006).
[8] G. Heliotis, G. Itskos, R. Murray, M. D. Dawson, I. M. Watson, and D. D. C. Bradley, Adv. Mater. **18**, 334 (2006).
[9] G. Itskos, G. Heliotis, P. G. Lagoudakis, J. Lupton, N. P. Barradas, E. Alves, S. Pereira, I. M. Watson, M. D. Dawson, J. Feldmann, R. Murray, and D. D. C. Bradley, Phys. Rev. B **76**, 035344 (2007).
[10] Q. Zhang, T. Atay, J. R. Tischler, M. S. Bradley, V. Bulović, and A. V. Nurmikko, Nat. Nanotechnol. **2**, 555 (2007).
[11] Y. Gao, A. Tonizzo, A. Walser, M. Potasek, and R. Dorsinville, Appl. Phys. Lett. **92**, 033106 (2008).
[12] K. Ema, M. Inomata, Y. Kato, H. Kunugita, and M. Era, Phys. Rev. Lett. **100**, 257401 (2008).
[13] N. Kawano, M. Koshimizu, and K. Asai, J. Phys. Chem. C **116**, 22992 (2012).
[14] H. Abassi, S. Jaziri, and R. Bennaceur, Physica (Amsterdam) **7E**, 686 (2000).
[15] R. J. Holmes, and S. R. Forrest, Phys. Rev. Lett. **93**, 186404 (2004).
[16] D. G. Lidzey, J. Wenus, D. M. Whittaker, G. Itskos, P. N. Stavrinou, D. D. C. Bradley, and R. Murray, J. Lumin. **110**, 347 (2004).
[17] R. J. Holmes, S. Kena-Cohen, V. M. Menon, and S. R. Forrest, Phys. Rev. B **74**, 235211 (2006).
[18] J. Wenus, R. Parashkov, S. Ceccarelli, A. Brehier, J.-S. Lauret, M. S. Skolnick, E. Deleporte, and D. G. Lidzey, Phys. Rev. B **74**, 235212 (2006).
[19] G. Lanty, S. Zhang, J. S. Lauret, E. Deleporte, P. Audebert, S. Bouchoule, X. Lafosse, J. Zuñiga-Pérez, F. Semond, D. Lagarde, F. Médard, and J. Leymarie, Phys. Rev. B **84**, 195449 (2011).
[20] V. Agranovich, H. Benisty, and C. Weisbuch, Solid State Commun. **102**, 631 (1997).
[21] J. Wainstain, C. Delalande, D. Gendt, M. Voos, J. Bloch, V. Thierry-Mieg, and R. Planel, Phys. Rev. B **58**, 7269 (1998).
[22] See Supplemental Material at http://link.aps.org/supplemental/10.1103/PhysRevLett.112.076401 for angle resolved room temperature photoluminescence data and simulations for the passive microcavity modes via the transfer matrix method.